ELSEVIER

Ultrasmall iron oxide nanoparticles: synthesis, surface modification, assembly, and biomedical applications

Cong Song, Wenjie Sun, Yunchao Xiao and Xiangyang Shi

State Key Laboratory for Modification of Chemical Fibers and Polymer Materials, College of Chemistry, Chemical Engineering and Biotechnology, Donghua University, Shanghai 201620, People's Republic of China

Ultrasmall iron oxide nanoparticles (USIO NPs) with a size <5 nm are a class of emerging nanomaterials. As a result of their intrinsic drawbacks related to poor colloidal stability, low r_1 relaxivity, and lack of functionality, various strategies have been adopted to synthesize USIO NPs with controllable sizes, to surface modify the particles with polymers, and to assemble them in combination with other nanoscale platforms. Here, we review recent progresses in the synthesis, surface modification, and self-assembly of USIO NPs to address key issues in their biomedical application in the field of cancer diagnosis and therapy, in particular magnetic resonance (MR) imaging, dual-modal or multimodal imaging, drug delivery, and theranostics.

Introduction

Over the past few decades, iron oxide nanoparticles (IO NPs) of various sizes have been synthesized and widely studied for diverse applications, in particular biomedical applications [1,2] including but not limited to drug delivery [3], MR imaging [4,5], and theranostics [6]. Among them, USIO NPs, with a diameter <5 nm, have attracted growing attention in biomedical fields as a result of their excellent biocompatibility, chemical stability, and tunable surface modifications [7–9]. Compared with normal IO NPs (size >5 nm), USIO NPs display reduced phagocytosis by macrophages, prolonged blood circulation time, and a dominant T_1-shortening effect [6,10]. The latter effect is particularly useful for MR imaging applications, especially when compared with gadolinium (Gd) chelate-based materials, which have problems resulting from Gd (III) leakage that causes renal systemic fibrosis, particularly in patients with abnormal kidney function [6,11,12]. Thus, a range of applications has been explored using USIO NPs, including MR imaging [13,14], multi-modality imaging [15,16], drug delivery [17,18], and theranostics [19,20].

To synthesize uniform IO NPs of suitable sizes, it is necessary to control the synthetic conditions (e.g., temperature, time, solvent, and reactant) [21,22]. An increasing number of routes to synthesize USIO NPs have been established and intensively explored for various application domains, including thermal decomposition, coprecipitation, hydrothermal or solvothermal synthesis, sol-gels, microemulsions, laser ablation, electrochemistry, and microwave-assisted methods [23,24]. For nanomedical research, USIO NPs have generally been conjugated with functional moieties or assembled to form desired superstructures via integration with inorganic materials, polymers, or biomacromolecules [25,26]. For instance, when conjugated with targeting molecules, USIO NPs can be applied as multifunctional nanoplatforms for targeted imaging and therapy of cancer and inflammation [27,28]. Although several recent reviews described the synthesis, assembly, and manipulation of IO NPs of different sizes for different biomedical applications [1,2,5,10,21,29,30], here we specifically focus on recent advances in the synthesis, assembly, and biomedical applications of USIO NPs. Rather than reviewing all aspects of USIO NPs, we introduce key developments in USIO NPs for use in biomedical applications.

Synthesis of USIO NPs

To generate USIO NPs of a uniform size and morphology, different chemical strategies have been used (Table 1), including coprecipitation, thermal decomposition, hydrothermal/solvothermal methods, and microemulsion (Fig. 1).

Corresponding author: Shi, X. (xshi@dhu.edu.cn)

https://doi.org/10.1016/j.drudis.2019.01.001

TABLE 1

Summary of the strategies used to generate USIO NPs of different sizes.

Synthetic strategy	NPs	Size (nm)	Refs
Coprecipitation	Fe_3O_4&γ-Fe_2O_3	2.0–15.0	[32]
	Fe_3O_4	4.5, 3.3	[7,33]
	Fe_3O_4	1.7, 2.2, 4.6	[34]
	γ-Fe_2O_3	2.0–15.0	[35]
Thermal decomposition	γ-Fe_2O_3	<3.0	[37]
	γ-Fe_2O_3	1.5–3.7	[38]
	Fe_3O_4	<4.0	[40]
Hydrothermal method	γ-Fe_2O_3	5.0	[43]
Solvothermal method	Fe_3O_4	1.9, 3.1, 4.2	[42]
	Fe_3O_4	2.8	[6,44]
Microemulsion method	Fe_3O_4	3.0–9.0	[45]
	γ-Fe_2O_3	3.5	[46]
Sol-gel method	Fe_3O_4&γ-Fe_2O_3	4.0	[47]
Microwave-assisted method	Sm^{3+}-doped γ-Fe_2O_3	4.5	[48]

Coprecipitation

Coprecipitation of Fe(II) and Fe(III) ions under basic conditions and elevated temperature is a classic method for the preparation of IO NPs. In this procedure, the size, morphology, and stability of IO NPs are closely related to: (i) composition of the reactants; (ii) molar ratio of ferrous and ferric ions; (iii) temperature of the reaction system; (iv) pH of the mixture solution; and (v) reaction time [31]. Jolivet *et al.* [32] synthesized IO NPs (2–15 nm) by adjusting the ionic strength and pH of the mixture solution. However, the iron precursor in this method was easily oxidized and deoxidized, resulting in unstable and uneven Fe_3O_4 NPs. To synthesize uniform IO NPs with an ultrasmall size, a high temperature coprecipitation method was established to create water-soluble and biocompatible NPs with a size of 4.5 ± 0.5 nm, in which poly (methacrylic acid) (PMAA-PTTM) was used as a stabilizer [7]. Li *et al.* [33] synthesized IO NPs with a smaller size (3.3 ± 0.5 nm) than that of the above particles by adopting the same process with a slight variation, whereby concentrated hydrogen chloride was selected to dissolve iron precursors before the addition of precipitating agents. In another report, Wang *et al.* [34] prepared high-quality USIO NPs in the presence of poly(acrylic acid) (PAA). Fe_3O_4 NPs of different sizes (1.7 nm, 2.2 nm, or 4.6 nm) were obtained by varying the reflux time periods (40 min, 60 min, or 120 min, respectively). Similarly, Li *et al.* prepared IO NPs with a diameter ranging from 2 to 15 nm via the aqueous coprecipitation of iron chlorides and auxiliary comonomers (MAA and acrylic acid) under alkaline conditions [35].

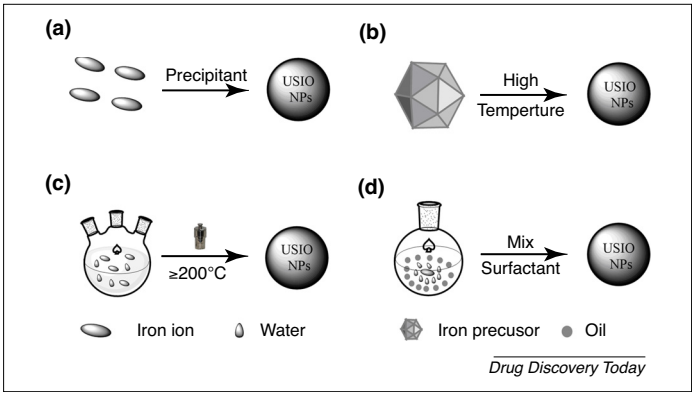

FIGURE 1

Schematic illustration of the formation of ultrasmall iron oxide nanoparticles (USIO NPs): **(a)** coprecipitation; **(b)** thermal decomposition; **(c)** hydrothermal method; and **(d)** microemulsion method.

Thermal decomposition

Thermal decomposition has been used to prepare IO NPs with accurate control of particle size and shape in a high-boiling organic solvent at a high temperature (usually 200 °C or higher) [8,36]. As an example, USIO NPs (γ-Fe_2O_3) <3 nm in diameter were synthesized via thermal decomposition using esters (diethylenglycolactetylacetonate and diethylenglycolpropionate) as a solvent or stabilizer to cover USIO NPs. The USIO NPs obtained were able to disperse uniformly in organic fluid [37]. In another study, USIO NPs (Fe_3O_4) were synthesized through thermal decomposition of iron-oleate complexes in the presence of oleyl alcohol and oleic acid. Interestingly, different sizes (1.5–3.7 nm) of USIO NPs were obtained by changing the reaction temperature and the oleyl alcohol:oleic acid ratio [38].

USIO NPs produced by thermal decomposition generally lack water dispersibility and biocompatibility because of the capped hydrophobic ligands, limiting their biomedical applications [39]. To solve this problem, researchers have optimized the thermal decomposition process used in their synthesis. For instance, to maintain homogenous heating, Uson *et al.* [40] designed metal-based microreactors with fast heat transfer to synthesize USIO NPs (<4 nm) in a continuous flow through thermal decomposition at high temperatures (>200 °C). In this multipurpose synthetic reactor, triethylene glycol was added to allow for the continuous production of USIO NPs and to endow the final USIO NPs with water-dispersibility and biocompatibility features.

Hydrothermal/solvothermal method

USIO NPs can also be synthesized by hydrothermal or solvothermal methods in either aqueous or organic solvents using a special container (e.g., autoclave) under elevated temperatures [41,42]. Compared with thermal decomposition, hydrothermal/solvothermal methods afford the creation of USIO NPs with water dispersibility and colloidal stability features. For instance, Gao *et al.* [43] established a facile and straightforward hydrothermal dephosphorylation approach to synthesize ultrasmall superparamagnetic γ-Fe_2O_3 NPs (5 nm) using 5′-guanosine monophosphate as a protecting agent. As an example of a solvothermal method, Shen *et al.* [42] synthesized highly water-dispersible USIO NPs with tailored sizes (1.9 nm, 3.1 nm, or 4.2 nm) by a one-pot method, in which trisodium citrate (Na_3Cit) was selected to stabilize USIO NPs *in situ*. Luo and Ma *et al.* [6,44] also used Na_3Cit as a grain growth inhibitor and a stabilizer in a polyol solution to synthesize USIO NPs under high temperature and high pressure conditions. The USIO NPs generated exhibited excellent long-term colloidal stability in various buffer solutions.

Microemulsion method

USIO NPs can be prepared using a microemulsion method. Darbandi *et al.* [45] mixed aqueous solutions of iron salt (0.1 M $FeCl_2$

and 0.2 M $FeCl_3$) and IGEPAL® CO-520 (an organic surfactant) in cyclohexane via vigorous stirring to form a microemulsion. Aqueous ammonia solution was then added to trigger the reaction at room temperature and IGEPAL® CO-520 stabilized the prepared NPs *in situ*. Uniformly sized crystalline USIO NPs with a spinel structure were obtained with a diameter ranging from 3 to 9 nm by adjusting the synthesis conditions [volume ratio of (organic solvent + water)/surfactant or stirring rate]. In another study, Vidal-Vidal *et al*. [46] chose water-in-oil microemulsion (cyclohexane/Brij-97/aqueous phase) to manufacture both coated and uncoated USIO NPs. The spherical particles capped with a monolayer of oleyl amine (or oleic acid) showed a narrow size distribution of 3.5 ± 0.6 nm, were crystalline, and had a high saturation magnetization.

Other methods

Other synthetic methods have also been explored to manufacture USIO NPs. Tadic *et al*. [47] produced highly crystalline USIO NPs using a sol-gel method in a silica matrix, with a sample size of ~4 nm without particle agglomeration. In addition, Lastovina *et al*. [48] utilized a microwave-assisted method to prepare rare earth metal ion Sm^{3+}-doped γ-Fe_2O_3 NPs with a size of 4.5 nm.

Surface modification of USIO NPs

Surface modification is a commonly used strategy to endow USIO-based NPs with good colloidal stability and versatility for biomedical applications [49,50]. Here, we summarize the main strategies used to modify the surface of USIO NPs.

Ligand exchange

Ligand exchange has been used for the surface modification of USIO NPs to improve their stability and water dispersibility. For instance, by means of a ligand exchange process, phosphate-functionalized polyethylene glycol (PEG) was utilized to modify the preformed oleic acid-stabilized USIO NPs for phase transfer to an aqueous solution [51]. The acquired USIO NPs showed high colloidal stability under various pH conditions, under ionic strength up to 2 M of NaCl, and under various buffer systems. In another study, Dolci and coworkers [52] reported the synthesis and physicochemical characterization of metal carbamato-functionalized USIO NPs. They first prepared oleate-coated USIO NPs via thermal decomposition and then modified the NPs with titanium-*N*,*N*-dialkylcarbamato [$Ti(O_2CNEt_2)_3$] through a ligand-exchange approach. The $Ti(O_2CNEt_2)_3$ coating did not affect the morphology or size of the USIO NPs. Meanwhile, the prepared Ti $(O_2CNEt_2)_3$-coated USIO NPs presented an increase in magnetization and more intense superparamagnetic behavior compared with oleate-coated USIO NPs. Moreover, the presence of residual O_2CNEt_2 groups on the surface of USIO NPs could be further modified with bioactive molecules for different biomedical applications. In addition, the Yang group [53] reported the synthesis of dopamine (DOPA)-coated USIO (Fe_3O_4@DOPA) NPs by ligand exchange. The Fe_3O_4@DOPA NPs were further modified with diethylenetriaminepentaacetic acid dianhydride (DTPA) through a condensation reaction for subsequent chelation with Gd(III) ions, resulting in Gd(III)-loaded USIO NPs with an enhanced longitudinal relaxivity (r_1) compared with single USIO NPs and Gd(III) complexes (Fig. 2a).

Covalent bonding

In addition to the ligand exchange method, surface modification of USIO NPs can also be realized by covalent bonding reactions [6,44]. For example, Luo *et al*. [6] first synthesized citrate-stabilized USIO NPs with a mean size of 2.8 nm through a solvothermal route. Then, the citrate-stabilized USIO NPs were modified with methoxy PEG amine (*m*PEG-NH_2) through a 1-(3-dimethylaminopropyl)-3-ethylcarbodiimide (EDC) coupling reaction between the carboxyl group of USIO NPs and the amine group of *m*PEG-NH_2. Moreover, the above citrate-stabilized USIO NPs could also be further modified with PEGylated arginylglycylaspartic acid (RGD) peptide with the other end of amine group through EDC coupling (Fig. 2b).

Other methods

USIO NPs have also been modified with various polymers or materials by other methods, such as reverse microemulsion and hydrophobic interactions. For instance, Iqbal *et al*. synthesized hydrophobic USIO NPs with a mean size of 4 nm [54] and then functionalized them with a SiO_2 shell using a reverse microemulsion method. The Fe_3O_4@SiO_2 USIO NPs obtained could be transferred to a hydrophilic aqueous phase and be rendered with enhanced biocompatibility because of the modification of the SiO_2 shell. Meanwhile, USIO NPs have also been modified with zwitterionic ligands by hydrophobic interactions to endow them with good antifouling properties [55–57]. As an example, Pombo-Garcia *et al*. [56] reported the preparation of USIO NPs modified with a zwitterionic polymer, poly(maleic anhydride-alt-1-decene) modified with 3-(dimethylamino)propylamine (PMAL) through hydrophobic interactions. The authors synthesized the oleic acid/oleyl alcohol-stabilized USIO NPs via thermal decomposition and then modified PMAL through hydrophobic interactions between the octyl chains of the PMAL and the hydrocarbon tails of oleic acid and oleyl alcohol.

Assembly of USIO NPs

In addition to the surface modification of USIO NPs, USIO NPs can be assembled with different materials to improve their physicochemical properties and to endow them with multifunctionalities. There are two main assembly methods: assembly of USIO NPs by *in situ* strategies and assembly of preformed USIO NPs.

Assembly of USIO NPs by in situ strategies

For the *in situ* chemical assembly of USIO NPs, matrix materials are usually required on which to load the USIO NPs. Mesoporous silica NPs (MSNs) and graphene nanosheets are commonly used matrix materials for the assembly of USIO NPs [41,58–61]. MSNs have a high surface:volume ratio, tunable nanometer-sized pores, and well-defined surface characteristics [10,62]. For instance, Wu *et al*. [59] reported a unique MSN-based platform with USIO NPs confined within the mesopore network. As shown in Fig. 2c, ferrocene was first loaded within mesopores of MSNs through a physical vapor infiltration (PVI) method (step 1). The pre-introduced ferrocene was then decomposed *in situ* to form highly dispersed USIO NPs confined within the MSNs (step 2). After treatment with H_2O_2 and H_2 (step 3), the USIO-MSNs generated were endowed with enhanced hydrophilicity and improved T_1-MR imaging performance (Fig. 2d). The developed USIO-MSNs can be

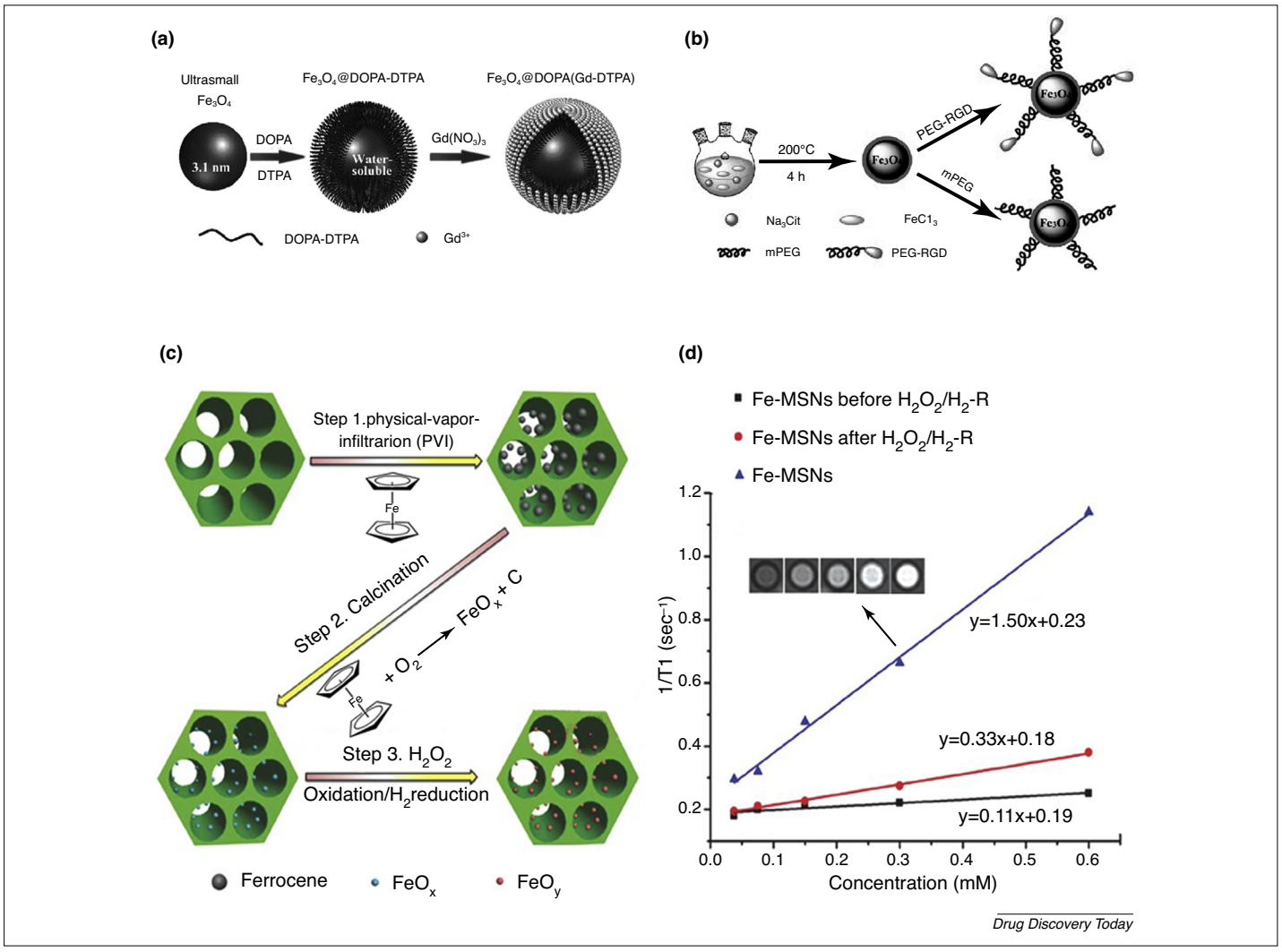

FIGURE 2

Surface modification and assembly of USIO NPs. Schematic illustration of **(a)** the preparation of Fe_3O_4@DOPA(Gd-DTPA) nanoparticles (NPs), **(b)** the preparation of Fe_3O_4-PEG-RGD and Fe_3O_4-*m*PEG NPs, and **(c)** the formation of ultrasmall iron oxide (USIO) NP-confined mesoporous silica NP (MSN) composites. **(d)** The inverse of T_1 versus Fe concentrations for Fe-MSNs before and after H_2O_2-O/H_2-R treatment. Reproduced, with permission, from Refs [53] (a), [6] (b), and [59] (d).

used for efficient T_1-weighted MR imaging and to load anticancer drugs for cancer chemotherapy.

Owing to their high surface:volume ratio and chemical stability, graphene nanosheets have also been used to assemble USIO NPs [60,63]. Chen *et al.* [61] decorated graphene oxide (GO) nanosheets with USIO NPs *in situ* via a hydrothermal method in the presence of GO, $FeCl_3{\cdot}6H_2O$, L-ascorbic acid, and dehydroascorbic acid. Subsequently, the USIO/GO hybrid formed was partially reduced to form the final product of USIO/G. Aside from the above two materials, carbon nanotubes (CNs) have also been used as a substrate for the assembly of USIO NPs *in situ* [64].

Furthermore, USIO NPs can also be assembled with metal NPs *in situ* [10,65,66]. For instance, Ivashchenko *et al.* [66] reported a unique one-step method to prepare self-organized silver/USIO NPs composites. In brief, self-organized Ag/USIO NPs were synthesized through regulated coprecipitation of silver ions (Ag^+) and iron ions (Fe^{3+} and Fe^{2+}) using ginger extract as a capping agent. The synthesized self-organized Ag/USIO NPs displayed a highly ordered hierarchical microstructure, and the sizes of Ag and USIO NPs in the formed hybrids were 5–25 nm and 1–3 nm, respectively. Moreover, the self-organized NPs displayed combined fluorescence and bactericidal properties, as well as MR contrast enhancement properties.

Assembly of preformed USIO NPs

In addition to the assembly of USIO NPs *in situ*, preformed USIO NPs can also be further assembled using different approaches [67,68]. The major difference between the two methods is that USIO NPs of the former are synthesized *in situ* during the assembly process, whereas the latter USIO NPs are synthesized first, followed by the assembly process.

MSNs can be used not only for the assembly of USIO NPs *in situ*, but also for the assembly of preformed USIO NPs [9,68]. For example, Lee *et al.* [9] reported assembled Fe_3O_4-MSN nanohybrids produced via immobilization of USIO NPs on the surface of MSNs. The authors first synthesized 2-bromo-2-methylpropionic (BMPA)-coated USIO

NPs and aminated MSNs, and then assembled the BMPA-coated USIO NPs onto the surface of MSNs via a direct nucleophilic substitution reaction between the terminal bromine groups of BMPA and the amine groups of the MSNs. The r_2 relaxivity of the assembled nanohybrids was 2.8-fold greater than that of separated USIO NPs, demonstrating the synergistic enhancement of the MR contrast. Gao *et al.* [68] constructed a drug delivery system based on radial mesoporous silica hybridized with multiscale IO NPs, doxorubicin (Dox), and folic acid (FA) for theranostics of breast cancer.

Dendrimers with abundant surface functional groups, monodispersity, and tunable nanoscale size could also be used to assemble performed USIO NPs. Yang *et al.* [69] reported the assembly of preformed USIO NPs onto generation 5 (G5) poly(amidoamine) (PAMAM) dendrimers through EDC coupling. The synthesized G5/Fe_3O_4 hybrid NPs displayed favorable water dispersibility, colloidal stability, and outstanding hemocompatibility. In another recent study [70], USIO NPs were reported to be assembled onto polyvinylidene fluoride (PVDF)-based textile fibers via melt-spinning. The formed USIO-labeled PVDF fibers were further knitted into vascular scaffolds for improved vessel replacement therapy applications. Wang *et al.* [16] designed a multimodal imaging contrast agent based on the assembly of USIO NPs (2.2 nm in diameter) onto the surface of Au nanocages (AuNCs) via an EDC coupling reaction.

In addition to assembly with other materials, USIO NPs could also be self-assembled through hydrophobic interactions, as demonstrated recently by Ling *et al.* [71]. In their work, pH-sensitive magnetic nanogrenades based on the self-assembly of USIO NPs were prepared by the co-assembly of hydrophobic USIO NPs (3 nm) and amphipathic polymeric ligands [chlorin e6 grafted poly(ethylene glycol)-poly(β-benzyl-L-aspartate derivatives]. The nanogrenades could target tumor sites via surface charge switching triggered by the acidic tumor microenvironment, and then *in situ* disassembled because of the repulsive forces.

Biomedical applications of USIO NPs

After surface modification or assembly through different approaches, USIO NPs or USIO NP-based hybrids have been applied for various biomedical applications, such as MR imaging, dual-modal and/or multimodal imaging, drug delivery, and theranostics [17,72–74].

MR imaging

MR imaging is a powerful, noninvasive imaging technique for the diagnosis of various diseases. Contrast agents used in MR imaging can be divided into two main categories: T_1-positive contrast agents and T_2-negative contrast agents [75,76]. IO NPs have been commonly used as contrast agents for MR imaging. The size of IO NPs influences their magnetic properties [77,78], whereby the magnetic movement of IO NPs decreases with decrease in their size because of the reduction of the volume magnetic anisotropy and spin disorders on their surfaces, resulting in the suppression of T_2 contrast effects and enhancement of T_1 contrast effects [42,79]. USIO NPs have been used as contrast agents for T_1 and T_2 MR imaging because of various advantages, including great sensitivity, good biocompatibility, and high relaxivity [67,68,80].

USIO NPs have been widely used for T_1-weighted MR imaging of cancer [6,44,74,81,82]. In a recent study, Ma *et al.* [44] reported the synthesis of zwitterion L-cysteine-coated USIO NPs for enhanced MR imaging of blood pools and tumors. The L-cysteine-coated USIO NPs formed via a PEG spacer (Fe_3O_4-PEG-Cys) displayed excellent antifouling properties, characterized by good protein resistance, decreased macrophage cellular uptake, and extended blood circulation time compared with USIO NPs coated with PEG. The half-life of the Fe_3O_4-PEG-Cys NPs (6.2 h) was three times longer than that of Fe_3O_4-*m*PEG NPs (2.1 h). With the noncompromised r_1 relaxivity (1.2 mM^{-1} s^{-1}) compared with Fe_3O_4-*m*PEG NPs (0.9 mM^{-1} s^{-1}) and good *in vivo* organ compatibility, the developed Fe_3O_4-PEG-Cys NPs were used as contrast agents for enhanced MR imaging of rat aorta and xenograft HeLa tumor model in mice.

To achieve specific targeted MR imaging of tumors, it is necessary to design and develop multifunctional USIO NPs bearing targeting ligands. One of the most widely used targeting ligands is RGD peptide, which can specifically bind $\alpha_v\beta_3$ integrin-overexpressing cancer cells [83]. In a recent study, Shi and coworkers [6] developed RGD-targeted USIO NPs for targeted T_1-weighted MR imaging of gliomas. The *in vivo* MR imaging studies indicated that mice bearing xenografted gliomas treated with RGD-targeted USIO NPs displayed a significantly enhanced MR signal:noise ratio compared with the group treated with the nontargeted USIO NPs. In another study, Wang *et al.* [53] synthesized Gd(III) complex-conjugated USIO [Fe_3O_4@DOPA(Gd-DTPA)] NPs with good cytocompatibility and hemocompatibility. Given the combination of Gd(III) and USIO NPs in one single nanoplatform, the prepared Fe_3O_4@DOPA(Gd-DTPA) NPs enhanced the longitudinal relaxivity (r_1) compared with USIO NPs and Gd(III) complexes. Therefore, the developed Fe_3O_4@DOPA(Gd-DTPA) NPs could be excellent potential candidates for T_1 MR imaging contrast agents by combining the T_1 effect of both USIO NPs and Gd(III) ions.

In addition to T_1 MR imaging applications, USIO-based NPs have also been used for T_2 MR imaging studies [2,69,72,73,84–86]. As an example, Wang *et al.* [84] synthesized bovine serum albumin (BSA)-functionalized USIO NPs with a mean size of 4.8 nm and a high r_2 relaxivity of 444.56 mM^{-1} s^{-1} that can be used for *in vivo* T_2-weighted MR imaging of tumors. In another study, Yang *et al.* [69] reported a method to assemble preformed citric acid-stabilized USIO NPs onto G5 PAMAM dendrimers linked with RGD peptide (G5.NHAc-RGD-Fe_3O_4 NPs) via an EDC coupling reaction. Given the clustering effect of USIO NPs with strong interparticle interactions, the USIO NPs did not display the expected prominent T_1-shortening effect, instead displaying an enhanced T_2-shortening effect with a higher r_2:r_1 ratio of 9.51. Hence, the developed G5.NHAc-RGD-Fe_3O_4 NPs could be used for targeted T_2-weighted MR imaging of C6 glioma cells *in vitro* and the xenografted tumor model *in vivo* (Fig. 3).

As described above, USIO NPs could be used for either T_1 or T_2 MR imaging applications. Therefore, for more accurate imaging applications, USIO NPs both with T_1 and T_2 MR imaging properties have been designed and synthesized [67,87]. For example, Hu *et al.* [87] synthesized water-soluble PEG-coated USIO NPs through a facile one-pot reaction. The PEG-coated USIO NPs presented an impressive saturation magnetization of 94 emu g^{-1}, a high r_1 relaxivity of 19.7 mM^{-1} s^{-1}, and a r_2:r_1 ratio of 2.0 at 1.5 T. T_1 and T_2 MR images indicated that the PEG-coated USIO NPs not only improved the surrounding water proton signals in the T_1 MR

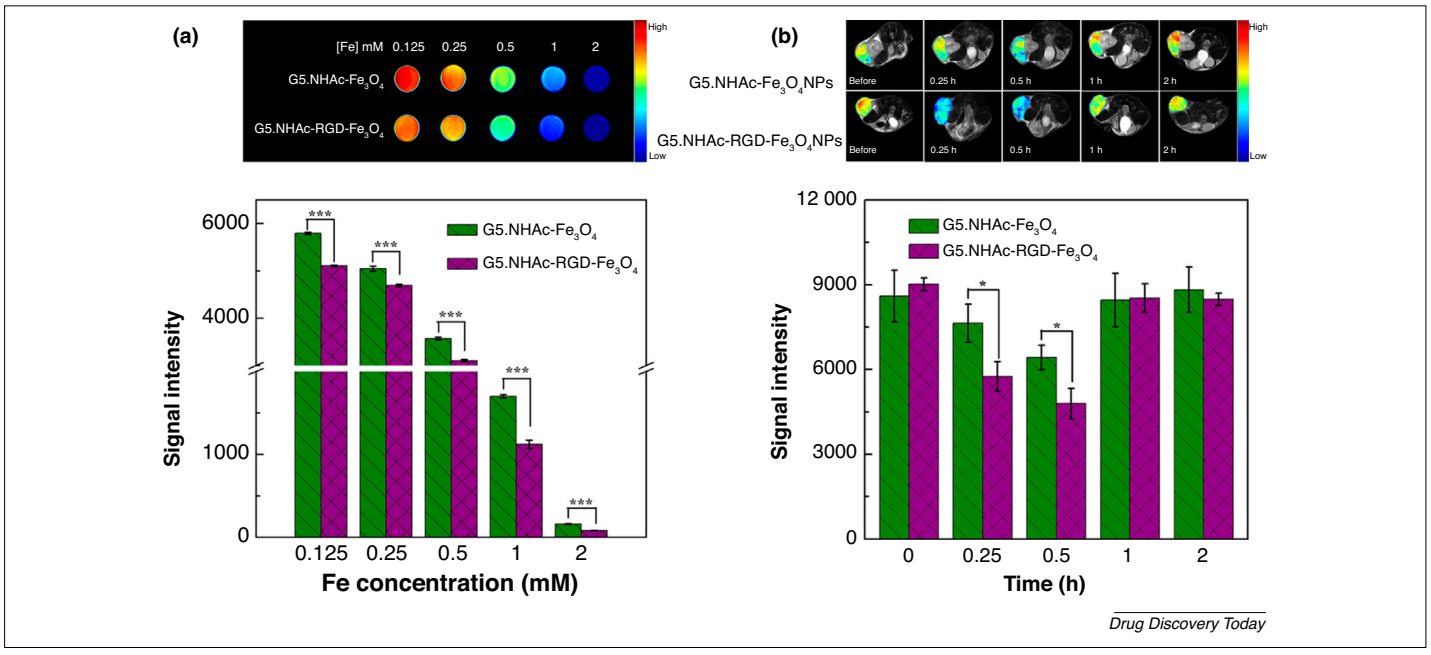

FIGURE 3

MR imaging of cancer cells *in vitro* and a xenografted tumor model *in vivo* using dendrimer/USIO NP nanohybrids. **(a)** T_2-weighted MR images and signal intensity of C6 cells treated with G5.NHAc-RGD-Fe_3O_4 NPs and G5.NHAc-Fe_3O_4 NPs for 4 h under different Fe concentrations; **(b)** *In vivo* T_2-weighted MR images and signal intensity of a xenografted C6 tumor model after intravenous injection of G5.NHAc-Fe_3O_4 NPs and G5.NHAc-RGD-Fe_3O_4 NPs (both containing 600 μg Fe) in 0.1 mL of phosphate buffered saline (PBS) solution separately at different times. Reproduced, with permission, from Ref. [69].

images, but also induced significant signal reduction in the T_2 MR images. These results demonstrated that PEG-coated USIO NPs could hold great promise for dual-modal T_1 and T_2 MR imaging applications.

Dual-modal or multimodal imaging

Given that each imaging modality has its own limitations and weaknesses, and none are able to provide complete structural and functional information independently [88], it is necessary to combine various imaging modes into one single nanoplatform to develop different dual-modal or multimodal contrast agents. Thus, various studies based on USIO NPs for dual-modal or multimodal imaging have been published [1,15,16,19,89,90].

In a recent study, Xue *et al.* [15] synthesized multifunctional USIO NPs for dual-modal MR and single-photon emission computed tomography (SPECT) imaging of tumor angiogenesis. In this work, USIO NPs with a mean size of 3.5 nm were created by a polyol method and then RGD peptide was modified on the surface of USIO NPs, followed by ^{99m}Tc labeling to acquire the final nanoprobe (^{99m}Tc-USIO-RGD NPs). The nanoprobe displayed good stability in PBS (pH 7.4), good r_1 relaxivity (8.2 mM^{-1} s^{-1}), reasonable T_2 contrast effects (r_2 = 20.1 mM^{-1} s^{-1}), and could specifically target $\alpha_v\beta_3$-positive cancer cells for combined dual-modal (T_1/T_2) MR imaging and tri-modal (T_1 MR/T_2 MR/SPECT) imaging of tumor angiogenesis *in vivo*.

In another study, Wang *et al.* [16] prepared an FA-targeted multimodal contrast agent based on USIO NPs and AuNCs through an EDC coupling reaction for tri-modal T_1 MR/T_2 MR/CT imaging of tumors. In this nanosystem, USIO NPs offered greatly enhanced MR signal contrast for both T_1 and T_2 MR imaging (r_1 = 6.26 mM^{-1} s^{-1}, r_2 = 28.12 mM^{-1} s^{-1}), whereas the Au NCs provided a strong X-ray attenuation property for CT imaging. *In vivo* studies revealed that the formed FA-AuNC@USIO NPs displayed an outstanding capability of selective accumulation in tumor tissues for tri-modal CT/T_1 MR/T_2 MR imaging of tumors.

Drug delivery

IO NPs have been proven to be an efficient nanoplatform for drug delivery applications [29,49]. Similarly, small-sized USIO NPs have also been explored for this purpose [3,17]. For example, Miller-Kleinhenz *et al.* [17] designed Dox-loaded USIO NPs (USIO-Dox) simultaneously conjugated with two targeting agents of Wnt/LRP5/6 and urokinase plasminogen activator receptor for effective inhibition of breast cancer cell invasion. In their study, a chemoresistant breast cancer tissue-derived tumor xenograft (PDX) model in nude mice was built up to evaluate the effect of conventional chemotherapy drugs and targeted USIO-Dox NPs. The dual targeted USIO-Dox NPs resulted in stronger tumor growth inhibition compared with nontargeted or single-targeted USIO-Dox NPs, validating the dual targeted USIO-Dox NPs as a valuable platform for enhanced drug delivery applications. In addition, Jeon *et al.* [3] developed a poly-paclitaxel/cyclodextrin-USIO (pPTX/CD-USIO) nanoassembly through multivalent host–guest interactions between β-cyclodextrin-conjugated USIO NPs and polymerized PTX for magnetically guided drug delivery. The clustering of USIO NPs in the nanoassembly enhanced the magnetization of USIO NPs, enabling their use for magnetic-guided drug delivery. Therefore, owing to the magnet-induced targeting effect, the developed pPTX/CD-USIO nanoassembly exhibited enhanced anticancer effects *in vitro* as well as *in vivo* compared with control groups.

Theranostics

Through surface modification or assembly with different methods, USIO NPs can be conjugated with therapeutic agents, such as chemotherapeutic drugs, photodynamic agents, and photothermal reagents, for MR imaging-guided theranostic applications [50,68,86,91–93].

For MR imaging-guided tumor chemotherapy, Gao *et al.* [68] reported a theranostic nanocomposite system based on MSNs hybridized with multiscale IO NPs, Dox, and FA for MR imaging and alternative magnetic field (AMF)-responsive chemotherapy of breast cancer. In this case, USIO NPs had a role as a T_2 contrast agent, and Fe_3O_4 NPs with a larger size were used to respond to the AMF. The prepared drug delivery system showed a high drug-loading efficiency of 86.2% and an excellent MR imaging contrast effect, with a high r_2 relaxivity of 308 mM^{-1} s^{-1}. Moreover, both *in vitro* and *in vivo* experiments demonstrated the potential of the prepared drug delivery system for MR imaging-guided chemotherapy of cancer.

In another study, a novel ultrasmall and highly stable Fe_3O_4@P-NPO/PEG-Glc@Ce6 nanoplatform was developed for dual-modal MR and optical imaging, improving tumor-targeting efficiency, and photodynamic therapy [86]. As shown in Fig. 4a, the polymer-coated USIO NPs (Fe_3O_4@P) were first conjugated with polyglycerol (NPO) dendrimers via EDC coupling reaction, and then connected with PEGylated glucose (Glc). Photosensitizer Ce6 was then coordinated with the Fe_3O_4@P-NPO/PEG-Glc to form the final product of Fe_3O_4@P-NPO/PEG-Glc@Ce6, which could generate singlet oxygen with the assistance of a near-infrared (NIR) laser irradiation to induce cell apoptosis. The small-sized Fe_3O_4@PNPO/PEG-Glc@Ce6 were efficiently taken up by tumor cells and could be used as a platform for dual-modal MR and/or optical imaging because of the coexistence of Fe_3O_4 NPs and the Ce6 dye, and for photodynamic therapy of tumor-bearing mice (Fig. 4b).

In addition, the Liu group [93] designed a USIO NP-based multifunctional nanoplatform via a layer-by-layer assembly approach for upconversion luminescence (UCL)/MR dual-modal imaging and magnetically targeted photothermal therapy (PTT). The prepared nanoplatform comprised a upconversion nanoparticle (UCNP) as the core, a layer of USIO NPs as the intermediate shell, and a thin layer of Au as the outer shell. At 2 h post intravenous injection, the tumor uptake of the platform under an external magnetic field was significantly higher than that without magnetic targeting according to UCL/MR dual-modal imaging and *in vivo* biodistribution data. *In vivo* PTT under a magnetic field was carried out on tumor-bearing mice at 2 h post injection of the nanoplatform. After NIR laser irradiation, all the tumors on mice were completely eliminated, and no tumor regrowth was observed in the treatment group over a course of 40 days. In a recent study, Lu *et al.* [94] developed a facile approach to synthesize dendrimer-stabilized gold nanoflowers (Au NFs) embedded with USIO NPs (Fe_3O_4/Au DSNFs) for multimodal T_1-weighted MR/CT/photoacoustic (PA) imaging and combination PTT/radiotherapy of tumors. With the embedment of USIO NPs,

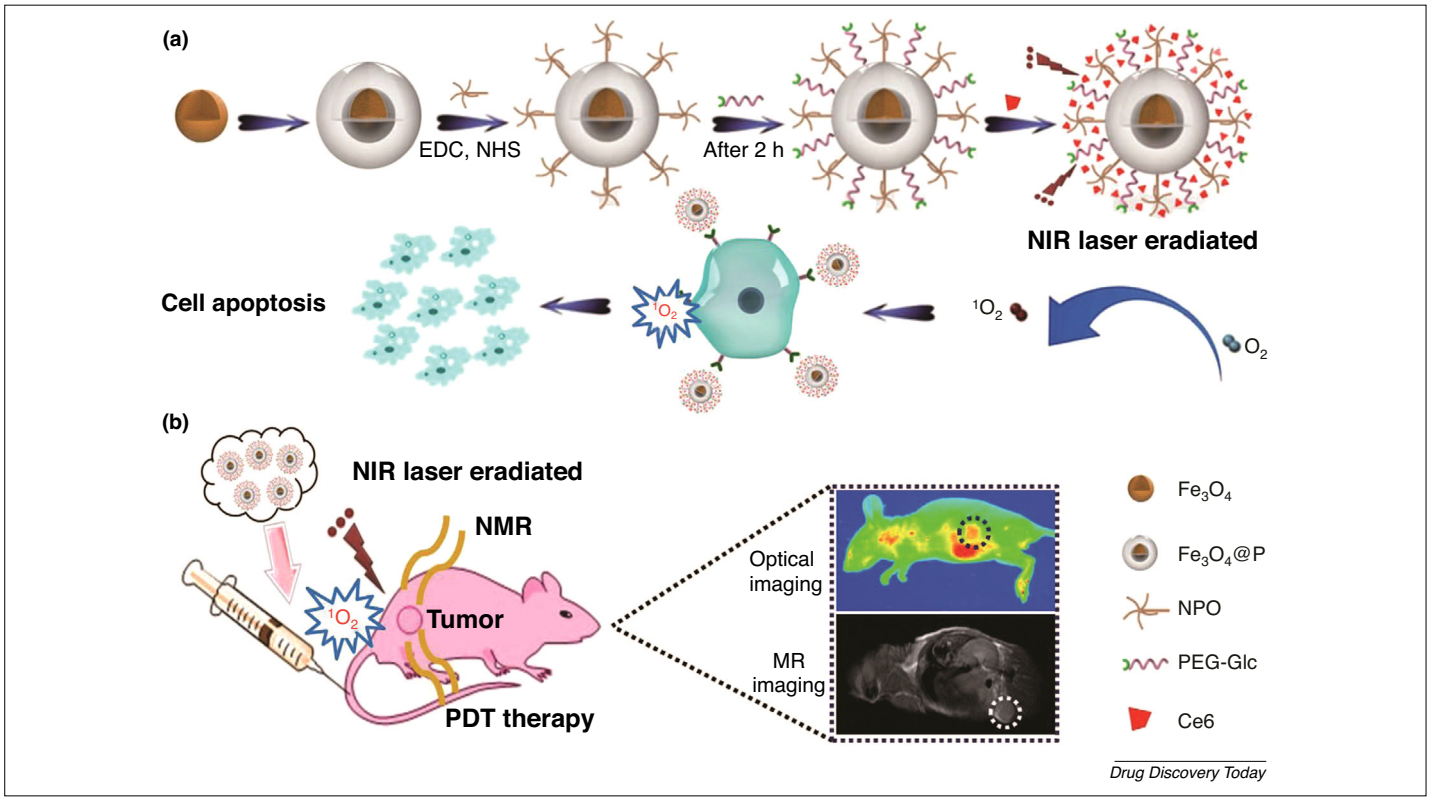

FIGURE 4

Schematic illustration of the formation of Fe_3O_4@P-NPO/PEG-Glc@Ce6 nanoprobe for dual-modal diagnosis and treatment. **(a)** Formation of an Fe_3O_4@P-NPO/PEG-Glc@Ce6 nanoprobe; **(b)** photodynamic therapy (PDT) and imaging in MGC-803 tumor-bearing mice. Reproduced, with permission, from Ref. [86]. Abbreviations: NIR, near-infrared; NMR, nuclear magnetic resonance.

the Fe_3O_4/Au DSNFs displayed higher r_1 relaxivity (3.22 mM^{-1} s^{-1}) than free USIO NPs, and enhanced NIR absorption properties, demonstrating their higher photothermal conversion efficiency (82.7%) compared with Au DSNFs without USIO NPs (63.1%). The developed Fe_3O_4/Au DSNFs could be used as an efficient theranostic nanoplatform for multimodal imaging-guided combination therapy of tumors for translational nanomedicine applications. These results indicate the promising potential of the prepared platform for cancer theranostics.

Concluding remarks and outlook

In summary, we have reviewed recent progresses in the development of USIO NPs and related nanohybrids for different biomedical applications. In particular, USIO NPs can be synthesized via different approaches, including coprecipitation, thermal decomposition, hydrothermal/solvothermal methods, and microemulsion. They can also be surface modified to endow them with improved antifouling properties and targeting specificity to a particular cancer type, as well as to be assembled with other matrix materials or self-assembled for improved functionality and stability. With the versatility of the preparation, surface modification, and assembly, the generated USIO NPs or the USIO NP-based nanohybrids can be used for MR (T_1/T_2) imaging, dual-modal or multimodal imaging, drug delivery, and theranostic applications.

Despite these significant achievements, further exploration in the field is still required. For instance, strategies used to improve the r_1 relaxivity of USIO NPs for T_1-weighted MR imaging applications could be further improved by developing new methods or new hybrid materials. More therapeutic approaches or drug types could be further combined with USIO NPs to achieve different theranostic applications of cancer, in particular for functional and/or structural imaging combined with precision diagnostics of cancer and for combinational therapy to overcome multidrug-resistant tumors. In addition, numerous issues remain to be solved for further clinical translation applications, such as large-scale production, quality control, and our currently poor understanding of their pharmacokinetics and long-term biosafety. Nevertheless, the future looks bright for the biomedical application of USIO NPs.

Acknowledgments

This research is financially supported by the National Natural Science Foundation of China (81761148028 and 21773026), the Fundamental Research Funds for the Central Universities, and the Science and Technology Commission of Shanghai Municipality (17540712000 and 15520711400).

References

1 Hu, Y. *et al.* (2018) Construction of iron oxide nanoparticle-based hybrid platforms for tumor imaging and therapy. *Chem. Soc. Rev.* 47, 1874–1900
2 Gao, J. *et al.* (2009) Multifunctional magnetic nanoparticles: design, synthesis, and biomedical applications. *Acc. Chem. Res.* 42, 1097–1107
3 Jeon, H. *et al.* (2016) Poly-paclitaxel/cyclodextrin-SPION nano-assembly for magnetically guided drug delivery system. *J. Control. Release* 231, 68–76
4 Li, J.C. *et al.* (2015) Facile synthesis of folic acid-functionalized iron oxide nanoparticles with ultrahigh relaxivity for targeted tumor MR imaging. *J. Mater. Chem. B* 3, 5720–5730
5 Li, J.C. *et al.* (2014) Hydrothermal synthesis and functionalization of iron oxide nanoparticles for MR imaging applications. *Part. Part. Syst. Charact.* 31, 1223–1237
6 Luo, Y. *et al.* (2015) RGD-functionalized ultrasmall iron oxide nanoparticles for targeted T_1-weighted MR imaging of gliomas. *Nanoscale* 7, 14538–14546
7 Li, Z. *et al.* (2008) Direct coprecipitation route to monodisperse dual-functionalized magnetic iron oxide nanocrystals without size selection. *Small* 4, 231–239
8 Gao, G. *et al.* (2010) Solvothermal synthesis and characterization of size-controlled monodisperse Fe_3O_4 nanoparticles. *J. Mater. Sci.* 45, 3483–3489
9 Lee, J.E. *et al.* (2010) Uniform mesoporous dye-doped silica nanoparticles decorated with multiple magnetite nanocrystals for simultaneous enhanced magnetic resonance imaging, fluorescence imaging, and drug delivery. *J. Am. Chem. Soc.* 132, 552–557
10 Ling, D. *et al.* (2015) Chemical synthesis and assembly of uniformly sized iron oxide nanoparticles for medical applications. *Acc. Chem. Res.* 48, 1276–1285
11 Abraham, J.L. and Thakral, C. (2008) Tissue distribution and kinetics of gadolinium and nephrogenic systemic fibrosis. *Eur. J. Radiol.* 66, 200–207
12 High, W.A. *et al.* (2007) Gadolinium is quantifiable within the tissue of patients with nephrogenic systemic fibrosis. *J. Am. Acad. Dermatol.* 56, 710–712
13 Usman, A. *et al.* (2017) Assessment of carotid plaque inflammation in diabetic and nondiabetic patients: an exploratory ultrasmall superparamagnetic iron oxide-enhanced magnetic resonance imaging study. *J. Stroke Cerebrovasc. Dis.* 26, 858–862
14 Chan, N. *et al.* (2014) Multidentate block-copolymer-stabilized ultrasmall superparamagnetic iron oxide nanoparticles with enhanced colloidal stability for magnetic resonance imaging. *Biomacromolecules* 15, 2146–2156
15 Xue, S.H. *et al.* (2015) ^{99}mTc-labeled iron oxide nanoparticles for dual-contrast (T_1/T_2) magnetic resonance and dual-modality imaging of tumor angiogenesis. *J. Biomed. Nanotechnol.* 11, 1027–1037
16 Wang, G.N. *et al.* (2016) Au nanocage functionalized with ultra-small Fe_3O_4 nanoparticles for Targeting T_1, T_2 dual MRI and CT imaging of tumor. *Sci. Rep.* 6, 28258
17 Miller-Kleinhenz, J. *et al.* (2018) Dual-targeting Wnt and uPA receptors using peptide conjugated ultra-small nanoparticle drug carriers inhibited cancer stem-cell phenotype in chemo-resistant breast cancer. *Biomaterials* 152, 47–62
18 Chandolu, V. and Dass, C.R. (2013) Treatment of lung cancer using nanoparticle drug delivery systems. *Curr. Drug Discov. Technol.* 10, 170–176
19 Das, M. *et al.* (2009) Biofunctionalized, phosphonate-grafted, ultrasmall iron oxide nanoparticles for combined targeted cancer therapy and multimodal imaging. *Small* 5, 2883–2893
20 Song, X.J. *et al.* (2014) Ultra-small iron oxide doped polypyrrole nanoparticles for *in vivo* multimodal imaging guided photothermal therapy. *Adv. Funct. Mater.* 24, 1194–1201
21 Jun, Y.W. *et al.* (2008) Nanoscaling laws of magnetic nanoparticles and their applicabilities in biomedical sciences. *Acc. Chem. Res.* 41, 179–189
22 Kim, D. *et al.* (2009) Synthesis of uniform ferrimagnetic magnetite nanocubes. *J. Am. Chem. Soc.* 131, 454–455
23 Wu, W. *et al.* (2016) Designed synthesis and surface engineering strategies of magnetic iron oxide nanoparticles for biomedical applications. *Nanoscale* 8, 19421–19474
24 Lastovina, T.A. *et al.* (2017) Microwave-assisted synthesis of magnetic iron oxide nanoparticles in oleylamine-oleic acid solutions. *Mendeleev Commun.* 27, 487–489
25 Sun, X. *et al.* (2012) Tuning exchange bias in core/shell FeO/Fe_3O_4 nanoparticles. *Nano Lett.* 12, 246–251
26 Shah, S.T. *et al.* (2017) Surface functionalization of iron oxide nanoparticles with gallic acid as potential antioxidant and antimicrobial agents. *Nanomaterials* 7, 306
27 Wu, E.X. *et al.* (2004) Applications of ultrasmall superparamagnetic iron oxide contrast agents in the MR study of animal models. *NMR Biomed.* 17, 478–483
28 Schuetz, C.A. *et al.* (2014) Differential stress reaction of human colon cells to oleic-acid-stabilized and unstabilized ultrasmall iron oxide nanoparticles. *Int. J. Nanomed.* 9, 3481–3498
29 Sun, W.J. *et al.* (2016) Dendrimer-based magnetic iron oxide nanoparticles: their synthesis and biomedical applications. *Drug Discov. Today* 21, 1873–1885
30 Li, J.C. *et al.* (2017) Aqueous-phase synthesis of iron oxide nanoparticles and composites for cancer diagnosis and therapy. *Adv. Colloid Interface Sci.* 249, 374–385
31 Hua, C.C. *et al.* (2008) Size-controlled synthesis and characterization of Fe_3O_4 nanoparticles by chemical coprecipitation method. *Sains Malays.* 37, 389–394
32 Jolivet, J.P. *et al.* (2002) Synthesis of iron oxide-based magnetic nanomaterials and composites. *C. R. Chim.* 5, 659–664
33 Li, Z. *et al.* (2012) Ultrasmall water-soluble and biocompatible magnetic iron oxide nanoparticles as positive and negative dual contrast agents. *Adv. Funct. Mater.* 22, 2387–2393

34 Wang, G.N. *et al.* (2014) One-step synthesis of water-dispersible ultra-small Fe_3O_4 nanoparticles as contrast agents for T_1 and T_2 magnetic resonance imaging. *Nanoscale* 6, 2953–2963
35 Li, K. *et al.* (2016) Surfactant-free emulsion polymerization stabilized by ultrasmall superparamagnetic iron oxide particles using acrylic acid or methacrylic acid as auxiliary comonomers. *Macromolecules* 49, 7609–7624
36 Park, S.J. *et al.* (2000) Synthesis and magnetic studies of uniform iron nanorods and nanospheres. *J. Am. Chem. Soc.* 122, 8581–8582
37 Milivojevic, D. *et al.* (2014) Magnetic properties of ultrasmall iron-oxide nanoparticles. *J. Alloys Compd.* 595, 153–157
38 Kim, B.H. *et al.* (2011) Large-scale synthesis of uniform and extremely small-sized iron oxide nanoparticles for high-resolution T_1 magnetic resonance imaging contrast agents. *J. Am. Chem. Soc.* 133, 12624–12631
39 Yu, W.W. *et al.* (2006) Aqueous dispersion of monodisperse magnetic iron oxide nanocrystals through phase transfer. *Nanotechnol* 17, 4483–4487
40 Uson, L. *et al.* (2018) Single phase microreactor for the continuous, high-temperature synthesis of <4 nm superparamagnetic iron oxide nanoparticles. *Chem. Eng. J.* 340, 66–72
41 Zhang, Z.P. *et al.* (2016) Ultrasmall Fe_2O_3 nanoparticles anchored on three-dimensional hierarchical porous graphene-like networks for high rate capability supercapacitors. *Chemelectrochem* 3, 1820–1826
42 Shen, L.H. *et al.* (2013) One-step synthesis of monodisperse, water-soluble ultra-small Fe_3O_4 nanoparticles for potential bio-application. *Nanoscale* 5, 2133–2141
43 Gao, G. *et al.* (2011) Synthesis of ultrasmall nucleotide-functionalized superparamagnetic gamma-Fe_2O_3 nanoparticles. *Crystengcomm* 13, 4810–4813
44 Ma, D. *et al.* (2017) Zwitterion-coated ultrasmall iron oxide nanoparticles for enhanced T_1-weighted magnetic resonance imaging applications. *J. Mater. Chem. B* 5, 7267–7273
45 Darbandi, M. *et al.* (2012) Nanoscale size effect on surface spin canting in iron oxide nanoparticles synthesized by the microemulsion method. *J. Phys. D Appl. Phys.* 45, 11
46 Vidal-Vidal, J. *et al.* (2006) Synthesis of monodisperse maghemite nanoparticles by the microemulsion method. *Colloids Surf. A* 288, 44–51
47 Tadic, M. *et al.* (2012) Highly crystalline superparamagnetic iron oxide nanoparticles (SPION) in a silica matrix. *J. Alloys Compd.* 525, 28–33
48 Lastovina, T.A. *et al.* (2018) Microwave-assisted synthesis of ultra-small iron oxide nanoparticles for biomedicine. *Mendeleev Commun.* 28, 167–169
49 Mahmoudi, M. *et al.* (2011) Superparamagnetic iron oxide nanoparticles (SPIONs): development, surface modification and applications in chemotherapy. *Adv. Drug Deliv. Rev.* 63, 24–46
50 Wang, Y. *et al.* (2018) Tumor-specific disintegratable nanohybrids containing ultrasmall inorganic nanoparticles: from design and improved properties to cancer applications. *Mater. Horiz.* 5, 184–205
51 Tromsdorf, U.I. *et al.* (2009) A highly effective, nontoxic T_1 MR contrast agent based on ultrasmall PEGylated iron oxide nanoparticles. *Nano Lett.* 9, 4434–4440
52 Dolci, S. *et al.* (2014) Ultrasmall superparamagnetic iron oxide nanoparticles with titanium-N,N-dialkylcarbamato coating. *Mater. Res. Express* 1 035401
53 Wang, L. *et al.* (2015) Gd(III) complex conjugated ultra-small iron oxide as an enhanced T_1-weighted MR imaging contrast agent. *J. Mater. Chem. B* 3, 1433–1438
54 Iqbal, M.Z. *et al.* (2015) Silica-coated super-paramagnetic iron oxide nanoparticles (SPIONPs): a new type contrast agent of T_1 magnetic resonance imaging (MRI). *J. Mater. Chem. B* 3, 5172–5181
55 Pombo-Garcia, K. *et al.* (2017) Zwitterionic modification of ultrasmall iron oxide nanoparticles for reduced protein corona formation. *Chempluschem* 82, 638–646
56 Pombo-Garcia, K. *et al.* (2016) Zwitterionic polymer-coated ultrasmall superparamagnetic iron oxide nanoparticles with low protein interaction and high biocompatibility. *ChemNanoMat* 2, 959–971
57 Biehl, P. *et al.* (2018) Synthesis, characterization, and applications of magnetic nanoparticles featuring polyzwitterionic coatings. *Polymers* 10, 91
58 Omar, H. *et al.* (2017) Biodegradable magnetic silica@iron oxide nanovectors with ultra-large mesopores for high protein loading, magnetothermal release, and delivery. *J. Control. Release* 259, 187–194
59 Wu, M. *et al.* (2014) Ultrasmall confined iron oxide nanoparticle MSNs as a pH-responsive theranostic platform. *Adv. Funct. Mater.* 24, 4273–4283
60 Zhang, S.H. *et al.* (2015) One-pot synthesis of ultra-small magnetite nanoparticles on the surface of reduced graphene oxide nanosheets as anodes for sodium-ion batteries. *J. Mater. Chem. A* 3, 4793–4798
61 Chen, Y. *et al.* (2013) Ultra-small Fe_3O_4 nanoparticle decorated graphene nanosheets with superior cyclic performance and rate capability. *Nanoscale* 5, 6797–6803
62 Mekaru, H. *et al.* (2015) Development of mesoporous silica-based nanoparticles with controlled release capability for cancer therapy. *Adv. Drug Deliv. Rev.* 95, 40–49
63 Deng, L. *et al.* (2016) Hybrid iron oxide-graphene oxide-polysaccharides microcapsule: a micro-matryoshka for on-demand drug release and antitumor therapy *in vivo*. *ACS Appl. Mater. Interfaces* 8, 6859–6868
64 Xu, J.X. *et al.* (2012) Controlled assembly of ultrasmall iron oxide nanoparticles on carbon nanotubes: Facile preparation and interfacially induced ferromagnetism. *Chem. Lett.* 41, 227–228
65 Ivashchenko, O. *et al.* (2018) Silver and ultrasmall iron oxides nanoparticles in hydrocolloids: effect of magnetic field and temperature on self-organization. *Sci. Rep.* 8, 4041
66 Ivashchenko, O. *et al.* (2017) Self-organizing silver and ultrasmall iron oxide nanoparticles prepared with ginger rhizome extract: Characterization, biomedical potential and microstructure analysis of hydrocolloids. *Mater. Des.* 133, 307–324
67 Zhou, H.G. *et al.* (2017) *In vivo* aggregation-induced transition between T_1 and T_2 relaxations of magnetic ultra-small iron oxide nanoparticles in tumor microenvironment. *Nanoscale* 9, 3040–3050
68 Gao, Q. *et al.* (2018) A theranostic nanocomposite system based on radial mesoporous silica hybridized with Fe_3O_4 nanoparticles for targeted magnetic field responsive chemotherapy of breast cancer. *RSC Adv.* 8, 4321–4328
69 Yang, J. *et al.* (2015) Conjugation of iron oxide nanoparticles with RGD-modified dendrimers for targeted tumor MR imaging. *ACS Appl. Mater. Interfaces* 7, 5420–5428
70 Mertens, M.E. *et al.* (2015) USPIO-labeled textile materials for non-invasive MR imaging of tissue-engineered vascular grafts. *Biomaterials* 39, 155–163
71 Ling, D.H. *et al.* (2014) Multifunctional tumor pH-sensitive self-assembled nanoparticles for bimodal imaging and treatment of resistant heterogeneous tumors. *J. Am. Chem. Soc.* 136, 5647–5655
72 Richards, J.M.J. *et al.* (2011) Abdominal aortic aneurysm growth predicted by uptake of ultrasmall superparamagnetic particles of iron oxide a pilot study. *Circ. Cardiovasc. Imaging* 4, 274–281
73 McBride, O.M.B. *et al.* (2015) MRI using ultrasmall superparamagnetic particles of iron oxide in patients under surveillance for abdominal aortic aneurysms to predict rupture or surgical repair: MRI for abdominal aortic aneurysms to predict rupture or surgery: the MA(3)RS study. *Open Heart* 2, e000190
74 Jia, Z.Y. *et al.* (2016) Active-target T_1-weighted MR imaging of tiny hepatic tumor via RGD modified ultra-small Fe_3O_4 nanoprobes. *Theranostics* 6, 1780–1791
75 Laurent, S. *et al.* (2008) Magnetic iron oxide nanoparticles: synthesis, stabilization, vectorization, physicochemical characterizations, and biological applications. *Chem. Rev.* 108, 2064–2110
76 Boros, E. *et al.* (2015) MR imaging probes: design and applications. *Dalton Trans.* 44, 4804–4818
77 Demortière, A. *et al.* (2011) Size-dependent properties of magnetic iron oxide nanocrystals. *Nanoscale* 3, 225–232
78 Wang, D. *et al.* (2012) Reduction on cogging torque in flux-switching permanent magnet machine by teeth notching schemes. *IEEE Trans. Magn.* 48, 4228–4231
79 Estelrich, J. *et al.* (2015) Nanoparticles in magnetic resonance imaging: from simple to dual contrast agents. *Int. J. Nanomed.* 10, 1727–1741
80 Sadat, U. *et al.* (2011) Ultrasmall superparamagnetic iron oxide-enhanced magnetic resonance imaging of abdominal aortic aneurysms—A feasibility study. *Eur. J. Vasc. Endovasc. Surg.* 41, 167–174
81 Branka, B.S. *et al.* (2018) Ultrasmall iron oxide nanoparticles: Magnetic and NMR relaxometric properties. *Curr. Appl. Phys.* 18, 141–149
82 Rui, Y.P. *et al.* (2016) Ultra-large-scale production of ultrasmall superparamagnetic iron oxide nanoparticles for T_1-weighted MRI. *RSC Adv.* 6, 22575–22585
83 Xie, J. *et al.* (2008) Ultrasmall c(RGDyK)-coated Fe_3O_4 nanoparticles and their specific targeting to integrin alpha(v)beta(3)-rich tumor cells. *J. Am. Chem. Soc.* 130, 7542–7543
84 Wang, Y.L. *et al.* (2017) Ultrasmall superparamagnetic iron oxide nanoparticle for T_2-weighted magnetic resonance imaging. *ACS Appl. Mater. Interfaces* 9, 28959–28966
85 Yar, Y. *et al.* (2018) Development of tailored SPION-PNIPAM nanoparticles by ATRP for dually responsive doxorubicin delivery and MR imaging. *J. Mater. Chem. B* 6, 289–300
86 Yin, T. *et al.* (2017) *In vivo* high-efficiency targeted photodynamic therapy of ultra-small Fe_3O_4@polymer-NPO/PEG-Glc@Ce6 nanoprobes based on small size effect. *NPG Asia Mater.* 9, e383
87 Hu, F.Q. *et al.* (2011) Facile synthesis of ultrasmall PEGylated iron oxide nanoparticles for dual-contrast T_1- and T_2-weighted magnetic resonance imaging. *Nanotechnology* 22, 245604
88 Jennings, L.E. and Long, N.J. (2009) 'Two is better than one'-probes for dual-modality molecular imaging. *Chem. Commun.* 3511–3524
89 Cho, B.B. *et al.* (2015) Synthesis and characterization of Ga-68 labeled Fe_3O_4 nanoparticles for positron emission tomography (PET) and magnetic resonance imaging (MRI). *J. Radioanal. Nucl. Chem.* 305, 169–178

90 Carron, S. *et al.* (2016) Ultrasmall superparamagnetic iron oxide nanoparticles with europium(iii) DO3A as a bimodal imaging probe. *Chem. Eur. J.* 22, 4521–4527
91 Feng, L. *et al.* (2017) A core-shell-satellite structured Fe_3O_4@g-C_3N_4-UCNPs-PEG for T_1/T_2-weighted dual-modal MRI-guided photodynamic therapy. *Adv. Healthc. Mater.* 6, 1700502
92 Dong, Y. *et al.* (2016) Polymer-lipid hybrid theranostic nanoparticles co-delivering ultrasmall superparamagnetic iron oxide and paclitaxel for targeted magnetic resonance imaging and therapy in atherosclerotic plaque. *J. Biomed. Nanotechnol.* 12, 1245–1257
93 Cheng, L. *et al.* (2012) Multifunctional nanoparticles for upconversion luminescence/MR multimodal imaging and magnetically targeted photothermal therapy. *Biomaterials* 33, 2215–2222
94 Lu, S.Y. *et al.* (2018) Dendrimer-stabilized gold nanoflowers embedded with ultrasmall iron oxide nanoparticles for multimode imaging-guided combination therapy of tumors. *Adv. Sci.* 1801612